CFD MODELLING OF PARTICLE SUSPENSION IN STIRRED TANKS

Alessandro Tamburini[a], Andrea Cipollina[a], Giorgio Micale[a], Alberto Brucato[a] and Michele Ciofalo[b]

[a] *Dipartimento di Ingegneria Chimica, Gestionale, Informatica, Meccanica - Università degli Studi di Palermo, Viale delle Scienze Edificio 6 - 90128 Palermo. Email: a.tamburini@unipa.it*

[b] *Dipartimento dell'Energia - Università degli Studi di Palermo, Viale delle Scienze Edificio 6 - 90128 Palermo.*

ABSTRACT

Mixing of solid particles into liquids in mechanically agitated vessels is a topic of primary importance for several industrial applications. A great deal of research efforts has been devoted so far to the assessment of the minimum impeller speed (N_{js}) able to guarantee that all particles are suspended. Conversely, only little attention has been paid to the evaluation of the amount of solid particles that are suspended at impeller speeds N lower than N_{js}, despite the fact that in a number of industrial applications agitation speeds smaller than N_{js} are actually adopted [1,2].

The present work deals with dense solid-liquid partial suspensions in baffled stirred tanks and particularly focuses on the prediction of the amount of suspended particles at a number of angular velocities by means of Computational Fluid Dynamics. An Eulerian-Eulerian Multi Fluid Model coupled with a standard k-ε turbulence model is adopted for CFD simulations. Both Sliding Grid and Multiple Reference Frame approaches are employed to simulate the impeller-tank relative rotation. The computational model is validated by comparison with purposely collected experimental data.

1. INTRODUCTION

Mixing of systems containing solid particles suspended in a liquid is required in a number of chemical and industrial processes, which are usually carried out in stirred tanks. Information on suspension quality is of great importance for the design and operation of solid-liquid stirred tanks.

Most industrial applications involving transport phenomena between particles and a liquid phase require that the active interfacial area is maximized. This means that the stirrer should guarantee the suspension of all particles, keeping at the same time an impeller speed not too high to ensure acceptable energy consumptions. The well known compromise between these two aspects is represented by the choice of the minimum impeller speed required for the complete off-bottom suspension of the solids in the vessel (N_{js}), a very important parameter for industrial mixing process design and optimization.

Actually, energy savings can sometimes counterbalance the loss of active interfacial area so that a number of industrial installations is actually operated at $N<N_{js}$. In this regard,

knowledge of the fraction of suspended particles at different impeller speeds could be very useful to perform such economical balances.

So far, most researchers have focused their attention on the evaluation of N_{js}, but only few efforts have been devoted to the assessment of the dependence of suspended particle fraction on impeller speed (*suspension curves).* Among these Brucato and Brucato [3] utilized a technique based on the "twin systems" concept [4] for the determination of the fraction of unsuspended solid particles at impeller speeds lower than N_{js}. This technique was considered reliable when the fraction of unsuspended solids is lower than 0.5, but too demanding in terms of experimental work. Conversely, Brucato et al. [5] and Micale et al. [6] proposed a novel technique, namely the Pressure Gauge Technique (*PGT*), able to assess the percentage of suspended solids in a stirred tank, at a given impeller speed, by means of pressure measurements on tank bottom.

To the authors' knowledge no CFD works aimed at predicting suspension curves exist in the open literature, although a few works dealt with CFD simulations of solid-liquid suspensions at impeller speeds lower than the minimum for complete suspension [7-12]. Most of these focused on the prediction of N_{js} rather than paying attention to fillets extent or fully exploring partial suspension conditions.

Scope of the present work was that of setting up an effective CFD model for partial suspension conditions and carrying out simulations with the aim of numerically predicting suspension curves. Experimental data were obtained by *PGT* [5,6] and subsequently employed for validating the CFD approach. The proposed CFD model was found to satisfactory predict suspension curves.

2. EXPERIMENTAL

The experimental system consisted of a cylindrical flat bottomed baffled tank (T = 0.19m, total liquid height H=T). A standard six-bladed Rushton turbine (D=T/2) set at T/3 from vessel bottom, was used for all suspension experiments. The impeller shaft was driven by a DC motor provided with a speed control loop. An optical tachometer was employed to independently measure the impeller rotational speed. Deionised water and glass ballottini with diameter ranging between 212 and 250 μm were employed. Measured particle density was 2480 kg/m^3. The solid particle loading was equal to 1.6 kg corresponding to an average solid weight fraction (ratio of solid mass to liquid mass) of 33.8% (w/w). Void fraction of the particle bed lying on the bottom (under no agitation conditions) was experimentally measured to be about 40%. In order to inspect particle loading and particle size dependences, runs with 0.8 kg (16.9% w/w) and 500-600 μm glass ballottini were also conducted.

PGT Apparatus and Fundamentals

A pressure gauge made of a simple inclined manometer was connected to a given point of the vessel bottom allowing pressure readings to be taken. This point was placed azimuthally midway between two subsequent baffles and radially midway between the axis and the lateral wall. A hole in the vessel bottom transmitted the local pressure value to a dead chamber directly connected to the pressure gauge.

At N=0 all particles rest still on the vessel bottom and the measured pressure is proportional to the liquid height inside the vessel. Conversely, when some particles are suspended, a

pressure increase is observed because their weight is now transferred to vessel bottom via a pressure increase. This increase is easily related to the amount of suspended particles.

Full details on the apparatus and the technique are available in literature [5,6].

3. MODELLING AND NUMERICAL DETAILS

All CFD simulations were carried out by using the commercial code CFX4.4 (AEA technology). The Eulerian-Eulerian Multi Fluid Model was adopted for the two-phase system simulation. According to it, the two phases are assumed to coexist at every point in space in the form of interpenetrating continua that share the same pressure field. The code solves the continuity and momentum equations for the two-phases separately and simultaneously. The coupling between the two phases is obtained through inter-phase exchange terms.

The two continuity equations are:

$$\frac{\partial}{\partial t}\left(r_\alpha \rho_\alpha\right) + \vec{\nabla}\cdot\left(r_\alpha \rho_\alpha \vec{U}_\alpha\right) = 0 \tag{1}$$

$$\frac{\partial}{\partial t}\left(r_\beta \rho_\beta\right) + \vec{\nabla}\cdot\left(r_\beta \rho_\beta \vec{U}_\beta\right) = 0 \tag{2}$$

where the subscripts α and β refer to the continuous and dispersed phases respectively, r is their volumetric fraction, ρ is density and U is mean velocity. Clearly,

$$r_\alpha + r_\beta = 1 \tag{3}$$

The momentum balance equations are:

$$\frac{\partial}{\partial t}\left(r_\alpha \rho_\alpha \vec{U}_\alpha\right) + \vec{\nabla}\bullet\left\{r_\alpha\left[\rho_\alpha \vec{U}_\alpha \otimes \vec{U}_\alpha - \left(\mu_\alpha + \mu_{t\alpha}\right)\left(\vec{\nabla}\vec{U}_\alpha + \left(\vec{\nabla}\vec{U}_\alpha\right)^T\right)\right]\right\} = r_\alpha\left(\rho_\alpha \vec{g} - \vec{\nabla}P\right) + \vec{M}_{\alpha,\beta} \tag{4}$$

$$\frac{\partial}{\partial t}\left(r_\beta \rho_\beta \vec{U}_\beta\right) + \vec{\nabla}\bullet\left\{r_\beta\left[\rho_\beta \vec{U}_\beta \otimes \vec{U}_\beta - \mu_\beta\left(\vec{\nabla}\vec{U}_\beta + \left(\vec{\nabla}\vec{U}_\beta\right)^T\right)\right]\right\} = r_\beta\left(\rho_\beta \vec{g} - \vec{\nabla}P\right) + \vec{M}_{\beta,\alpha} \tag{5}$$

In these equations, g is gravity acceleration, μ is viscosity, μ_t is turbulent viscosity, P is pressure and M is momentum inter-phase transfer term.

The standard k-ε turbulence model was adopted to account for the turbulence of the continuum phase, while no turbulent viscous terms were considered for the solid phase. Simulations were carried out at different impeller speeds even at impeller speeds much lower than N_{js} when a lot of particles lie on vessel bottom. In such conditions resting particles are surrounded by other resting particles, thus being practically unaffected by turbulent viscous stresses. Therefore, the inclusion of turbulent viscosity in the momentum balance equation of the particle phase would have led to a strong overestimation of the amount of suspended particles. In this regard, the adoption of the homogeneous k-ε turbulence model (which also accounts for the turbulent viscous stresses for the particle phase) was found to provide very large overestimation of the suspended solid fraction, even at very low impeller speeds (i.e. when most particles should lie motionless on the bottom as sediments) [13].

Interactions between the two phases were directly modelled only by inter-phase drag force terms within the momentum equations (two-way coupling):

$$\vec{M}_{\alpha\beta} = -\vec{M}_{\beta\alpha} = C_{\alpha\beta}\left(\vec{U}_\beta - \vec{U}_\alpha\right) = \left[\frac{3}{4}\frac{C_D}{d_p} r_\beta \rho_\alpha \left|\vec{U}_\beta - \vec{U}_\alpha\right|\right]\left(\vec{U}_\beta - \vec{U}_\alpha\right) \quad (6)$$

where $C_{\alpha\beta}$ is inter-phase drag coefficient C_D is drag coefficient and d_p is particle diameter. Other inter-phase momentum exchange terms such as Basset force, virtual mass force and lift force are generally considered less important and consequently neglected [14].

It may be worth noting that the presence of a still sediment with a high local value of particle concentration gave rise to numerical convergence difficulties that practically inhibited the adoption of approaches such as the Granular Kinetic Theory or the Solid Pressure Model. When particles lie still on the bottom under packed conditions, the action of these two approaches may be crucial: they model particle normal stresses guaranteeing that the maximum packing of solid particles is not exceeded during simulations. In the present work the over-packing issue has been tackled by adopting the *Excess Solid Volume Correction* (*ESVC*) algorithm [15] (described later on). In practice, particle–particle interactions were neglected everywhere but in the sediment, where these were somewhat accounted for by the adoption of the *ESVC* algorithm.

The SIMPLEC algorithm was adopted to couple pressure and velocity. The hybrid-upwind discretization scheme was used for convective terms.

The structured grid chosen for simulations encompassed 53,760 cells distributed as 24 × 70 × 32 along the azimuthal, axial and radial direction respectively. Given the symmetry of the system, only half of the tank was simulated and two periodic boundaries were imposed along the azimuthal direction. The computational grid was finer in the proximities of the impeller where the largest gradients of the flow variables are expected.

This coarse grid was used in order to keep computational needs low. However, an eight times finer grid (430,080 cells) 48×140×64 (azimuthal×axial×radial) was also used to address the grid-dependence issue.

As far as the initial condition for all simulations is concerned, all particles were placed on the tank bottom with a initial volume fraction of 0.60 v/v , corresponding to the experimentally assessed maximum packing ($r_{\beta\text{-packed}}$).

Both transient and steady state simulations were carried out.

Transient simulations were performed by adopting the Sliding Grid (SG) algorithm to simulate the impeller-baffles relative motion. The time step employed for the simulations was equal to the time needed to rotate by a computational cell. For all the transient cases, 100 revolutions were found to be more than sufficient to reach steady state conditions. Therefore, for the coarse grid case, 4,800 time steps were required for completing each simulation. The number of iterations per time step was set to 30 with the aim of allowing residuals to settle before passing to the next time step as well as to enhance the number of times (per time step) in which the ESVC algorithm acts.

As far as steady state simulations are concerned, the multiple reference frame (MRF) approach was adopted. In this case 8,000 iterations were found to be sufficient for allowing variable residuals to settle to very low and negligible values for all the investigated cases.

Notably, simulations where impeller speed was high were found to require a higher number of total time steps (SG simulations) as well as higher number of total iterations (MRF simulations).

Drag Coefficient C_D

Particle drag coefficient C_D was considered as being variable in each cell in relation to the slip velocity between phases: C_D is calculated by the Clift et al. correlation [16] where the cell slip velocity was used for the Reynolds number calculation:

$$C_D = \frac{24}{\mathrm{Re}_p}\left(1 + 0.2\,\mathrm{Re}_p^{0.63}\right) \tag{7}$$

This approach is named in the followings as $C_{D\text{-}slip}$.

In order to account for free-stream turbulence influence upon inter-phase drag, two different correlations were implemented and tested: Brucato et al. [17] and Pinelli et al. [18] correlations:

$$C_{D,turb}^{Brucato} = C_D\left[1 + 8.67\times10^{-4}\left(\frac{d_p}{\lambda}\right)^3\right] \tag{8}$$

$$C_{D,turb}^{Pinelli} = C_D\left[0.6 + 0.4\tanh\left(16\frac{\lambda}{d_p} - 1\right)\right]^{-2} \tag{9}$$

where λ is Kolmogorov length scale, given by:

$$\lambda = \left[\left(\mu_\alpha / \rho_\alpha\right)^3 / \varepsilon\right]^{(1/4)} \tag{10}$$

where the turbulent dissipation ε is directly obtained by the turbulence model.

The relevant approaches will be referred to as $C_{D\text{-}turb}$-Brucato and $C_{D\text{-}turb\text{-}Pinelli}$ .The C_D coefficient of equations 8 and 9 is calculated by equation 7.

Excess Solid Volume Correction Algorithm (ESVC)

In order to avoid $r_{\beta\text{-}packed}$ to be exceeded during simulations, an ad-hoc algorithm, named *Excess Solid Volume Correction* [15], was implemented inside the User Fortran subroutine USRCVG of the CFX4.4 code. This correction operates as *a posteriori* redistribution of the solid volume in excess for each cell where the volume fraction exceeds $r_{\beta\text{-}packed}$. In the present version, it is applied at the end of each iteration of the SIMPLEC algorithm inside an iterative procedure. More precisely, it works iteratively either two hundreds times or until the total mass which exceeds $r_{\beta\text{-}packed}$ is reduced to one hundredth of its initial value. The algorithm rearranges the volume fraction distribution and ensures the excess of solids to be carried towards cells where no excess is present. It is worth noting that the *ESVC* algorithm effects at each iteration were always small, with total transferred mass below 2% in the worst cases.

Unsuspended Solids Criterion (USC)

It is clearly necessary to establish a criterion for correctly distinguishing suspended and unsuspended particles. According to *PGT* fundamentals, particles can be considered suspended when they move and lift off the vessel bottom thus contributing to the increase of apparent suspension mean density.

Solid particles laying motionless on the bottom show the maximum volumetric fraction $r_{\beta\text{-}packed}$ as their local volumetric fraction [7]. As a consequence, the criterion adopted was that all particles in cells with $r_\beta \geq r_{\beta\text{-}packed}$ were considered as being unsuspended. In addition, a suitable binary scalar named *sedim* was purposely prepared in order to allow 3-D visualizations of the sediment during post-processing: if particles inside a cell are considered as unsuspended, the scalar *sedim* is given a value of 1.0, otherwise it is equal to 0.0.

Notably, this criterion could underestimate the amount of unsuspended particles as some particles might stay on the bottom isolated from each other, but these are likely to be a few, so the relevant amount is low and can be neglected. It may be anticipated that in relation to the modus operandi of this criterion, a finer grid may be expected to result into a more precise estimation of the unsuspended solids.

Grid Dependence

A grid dependence check of computational results was performed for the case of 212-250 μm glass ballottini particles with mean solid concentration of 33.8%$^{w/w}$. Results concerning the coarse (53,760) and fine (430,080) computational grids are shown in Fig.1. As it can be seen, the suspended solid fraction data predicted by employing the fine grid is slightly lower than the corresponding coarse grid results, especially at intermediate impeller speeds. This is at least partially an outcome of the above described suspended solids criterion, which is bound to underestimate unsuspended solids the larger the computational cells. However, the extent of such discrepancies were judged to be small enough to make the coarse grid acceptable, for the purposes of the present work, in view of the large computational savings.

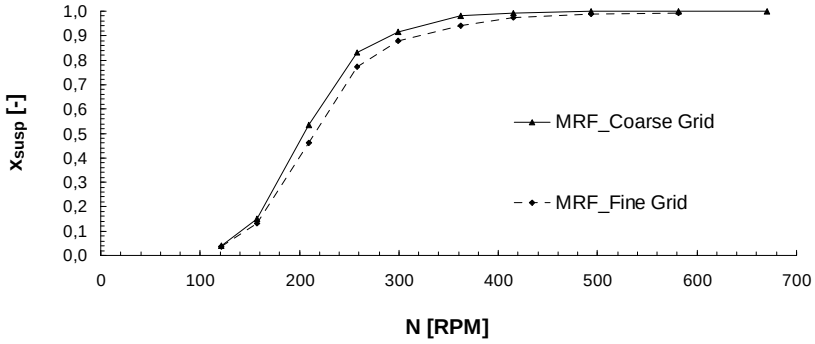

Figure 1. Comparison of MRF simulations (with $C_{D\text{-}turb\text{-}Brucato}$) carried out with two different computational grids for the case of 212-250 μm glass ballottini particles with a solid loading of 33.8%$^{w/w}$.

4. RESULTS AND DISCUSSION

Typical experimental results are shown in Fig.2, where it can be seen that the typical 'sigmoidal' trend found by Brucato et al. [5] and Micale et al. [6] is obtained.

Particle suspension was found to be higher with smaller particles and lower particle loadings, as expected. In addition, in the case of 550 μm particles, suspension occurs in a wider range of impeller speeds. Further details and discussion on experimental suspension curves can be found in Brucato et al. [5] and are not reported here for the sake of brevity.

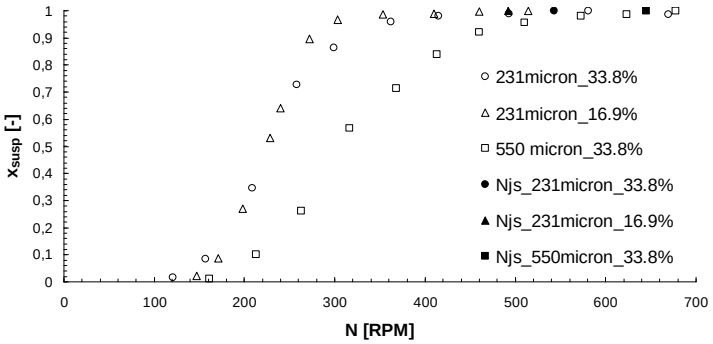

Figure 2. Experimental suspension curves for the following cases: ○ 212-250 μm glass ballottini particles with a solid loading of 33.8%$^{w/w}$; ∆ 212-250 μm glass ballottini particles with a solid loading of 16.9%$^{w/w}$; □ 550-600 μm glass ballottini particles with a solid loading of 33.8%$^{w/w}$. Solid geometric symbols indicates the relevant N_{js} values assessed by Zwietering's correlation [19]

In Fig. 3 fractional suspensions predicted by CFD-SG simulations are compared with the relevant experimental data. As it can be seen, despite the suspension criterion simplicity, simulation results appear to be in good agreement with experiment. As a matter of fact, they show the same "sigmoidal" trend and are close to the corresponding experimental data, although a slight overestimation can be observed, especially at intermediate impeller speeds. In the same figure two different approaches are compared: $C_{D\text{-}slip}$ and $C_{D\text{-}turb\text{-}Brucato}$. No significant differences are found between the two, as in this case particle diameter is rather small, which leads to relatively small increases of C_D . Namely at 200rpm $C_{D\text{-}turb\text{-}Brucato}$ / C_D =1.05 while $C_{D\text{-}turb\text{-}Pinelli}$ /C_D=1.01) and similar results are consequently obtained.

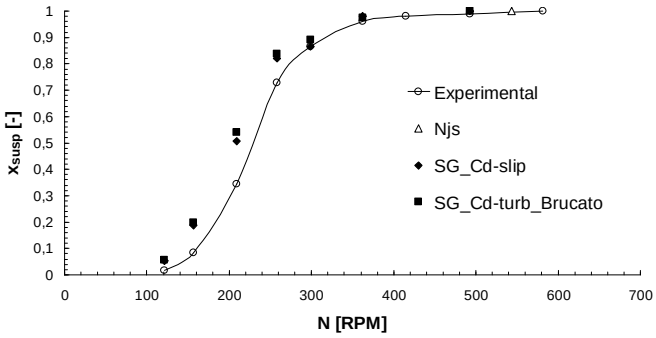

Figure 3. Simulated vs experimental suspension curve for the case of 212-250 μm glass ballottini particles with a solid loading of 33.8%$^{w/w}$. N_{js} was calculated by Zwietering's correlation [18].

In Fig.4 contour plots of r_β for the same case are reported: as it can be seen, at the lowest agitation speed (157rpm) almost all particles lay on vessel bottom; at 258rpm, many of them are suspended but are unable to reach the highest part of the tank; finally, at 493rpm suspension is very near to be complete and particles distribute following the liquid main flow and describing the typical double loop configuration.

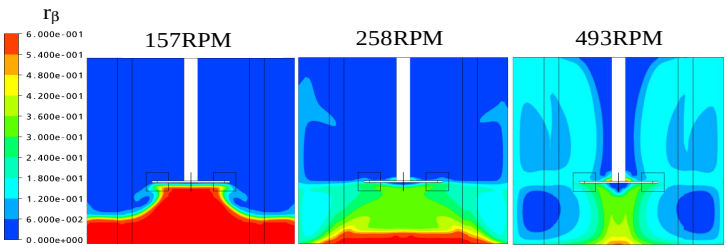

Figure 4. Contour plots of solid volumetric fractions on a vertical diametrical plane at three different impeller speeds for the case of 231 μm ballottini particles at 33.8%$^{w/w}$.

Fig.5 refers to the same cases described in Fig.4, and shows the iso-volume where the scalar *sedim* is equal to one. Such volume practically corresponds to the 3-D visualization of the sediment estimated by simulations. As Fig.5 shows, the amount of sediment is reduced by increasing impeller rotational speed. Particularly, at 258rpm the sediment provided by simulations shows a particular shape which is in agreement with experimental observation. Impeller rotates counter-clockwise and near the lateral wall a sediment is present only in the trailing side of the baffles, as it can be seen.

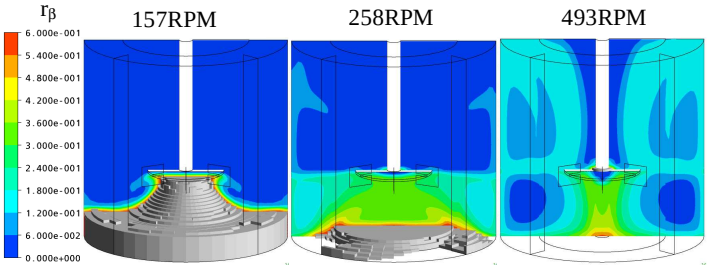

Figure 5. 3-D scalar *sedim* plot upon contour plots of solid volumetric fractions on a vertical diametrical plane at three different impeller speeds for the case of 231 μm ballottini particles at 33.8%$^{w/w}$.

SG (transient) simulation results are compared with MRF (steady-state) approach in Fig.6. It can be seen that practically identical results are obtained, confirming that the MRF approach may be conveniently adopted, in view of its large computational savings.

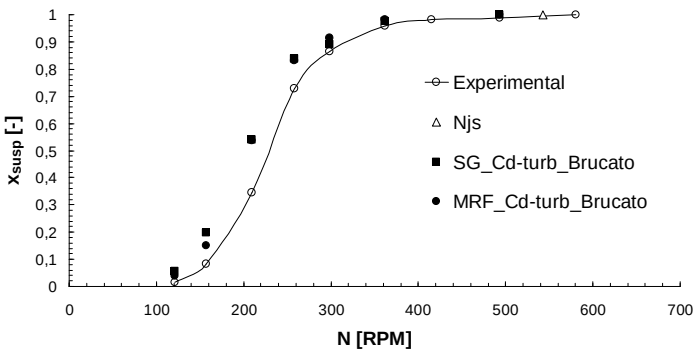

Figure 6. Comparison of SG and MRF simulations with experimental data for the case of 212-250 μm glass ballottini particles with a solid loading of 33.8%$^{w/w}$. N_{js} was calculated by Zwietering's correlation [18].

Also in the case of lower particle loading, such as that shown in Fig.7, simulation results follow quite well experimental data, as expected on the basis of the previous results. Predicted fractions of suspended solids are close enough to experiment, though a slight overestimation can be observed especially at the lowest impeller speeds. This might depend on experimental inaccuracies, as the PGT technique is admittedly less accurate at low fractional suspension values [6]. In any case, this region is not bound to be of interest for practical applications, being any likely industrial interest rather on the almost-complete suspension conditions.

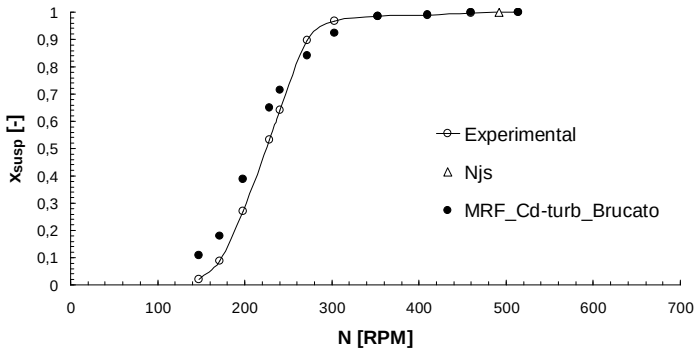

Figure 7. MRF simulations versus experimental data for the case of 212-250 μm glass ballottini particles with a solid loading of 16.9%$^{w/w}$. N_{js} was calculated by Zwietering's correlation [18].

As concerns particles size effects in Fig.8 experimental data and relevant simulations are reported for larger particles (500-600 μm). Larger particle size (and consequently higher impeller speed for the achieving of complete suspension conditions) give rise to higher d_p/λ ratio, therefore leading to greater influence of free-stream turbulence on particle drag coefficient. Neglecting such influence provides inconsistent results as the $C_{D\text{-}slip}$ simulation results (diamonds in Fig.7) show. Even at very high impeller speeds, $C_{D\text{-}slip}$ simulation results seem to predict that the fraction of suspended solid particles does not reach, nor asymptotically approach, the desired unitary value, as if complete suspension was impossible to achieve. As far as $C_{D\text{-}turb\text{-}Brucato}$ and $C_{D\text{-}turb\text{-}Pinelli}$ simulations are concerned, they clearly provide different enhancements of C_D , especially at the highest impeller speeds (i.e smaller λ and higher ratio d_p/λ). For instance at 678rpm the ratio $C_{D\text{-}turb\text{-}Brucato}$ to C_D is 14.87 while the ratio $C_{D\text{-}turb\text{-}Pinelli}$ to C_D is equal to 4.63. Observing Fig.8 data, it can be stated that experimental data are much better matched by the $C_{D\text{-}turb\text{-}Pinelli}$ (eq.9) approach.

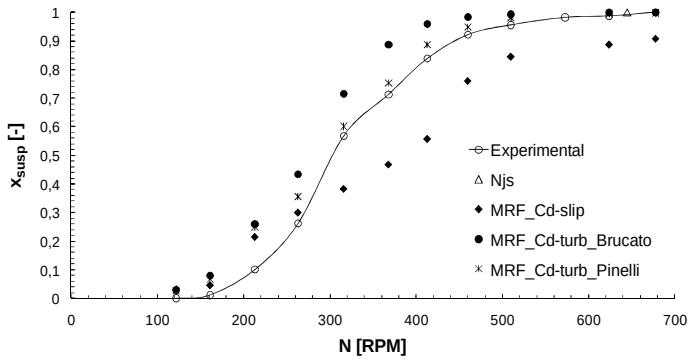

Figure 8. Comparison of different MRF simulation approaches with experimental data for the case of 500-600 μm glass ballottini particles with a solid loading of 33.8%$^{w/w}$. N_{js} was calculated by Zwietering's correlation [18].

5. CONCLUSIONS

Partial to complete suspension regime of dense solid-liquid suspensions within a flat bottomed fully baffled vessel stirred by a standard Rushton turbine was investigated by means of Computational Fluid Dynamics. Aim of the present work was to numerically predict suspension curves, i.e. the dependence of the fraction of unsuspended solids on the impeller speed.

RANS simulations were performed by adopting an Eulerian-Eulerian Multi Fluid Model framework with the help of the commercial code CFX4.4.

Two different correlations were implemented and tested in order to account for the effect of liquid free stream turbulence on drag coefficient.

The SG and MRF approaches were compared and no significant differences were found. Grid dependence was found to be acceptable.

Experimental data were purposely collected by means of the Pressure Gauge Technique in order to validate simulation results. Different particle sizes and concentrations were investigated.

Comparison between CFD predictions and all experimental data collected resulted in a very good agreement, despite the simple modelling approaches adopted.

Notably, taking into account the influence of turbulence on particle drag was found to be necessary in order to match simulations and experiment, especially for the largest particles.

Table 1. Nomenclature.

U	velocity (ms^{-1})
T	tank diameter (m)
H	liquid height (m)
D	impeller diameter (m)
g	gravitational constant (ms^{-2})
P	pressure (Nm^{-2})
r	volumetric fraction (-)
M	inter-phase term (Nm^{-3})
$C_{\alpha\beta}$	inter-phase drag term ($Kg\ m^{-3}s^{-1}$)
C_D	drag coefficient (-)
d_p	particle mean diameter (m)
N	rotational impeller speed (rpm)
N_{js}	just suspension impeller speed (rpm)
Re_p	particle Reynolds number (-)
k	turbulent kinetic energy ($m^2\ s^{-2}$)
x_{susp}	fraction of suspended solids
Greek letters	
μ	viscosity (Pa s)
ρ	density ($Kg\ m^{-3}$)
λ	Kolmogorov length (m)
ε	turbulent dissipation ($W\ Kg^{-1}$)
Subscripts	
α	liquid phase
β	solid phase
t	turbulent

ACKNOWLEDGEMENTS

This work was carried out under financial support by Ministero dell'Istruzione, dell'Università e della Ricerca, PRIN-2006 contract n° 2006091953_004.

REFERENCES

1. Oldshue, J. Y., (1983). *Fluid Mixing Technology*, Chapter 5, McGraw-Hill, New York, NY.

2. Rieger, F., Ditl, P., Havelkova, O., (1988). Suspension of solid particles–concentration profiles and particle layer on the vessel bottom. *Proceedings of the 6th European Conference on Mixing*, Pavia, Italy, 24-26 May, 251-258.

3. Brucato, A. and Brucato, V., (1998). Unsuspended mass of solid particles in stirred tanks. *Can. J. Chem. Eng.*, **76**, 420-427.

4. Brucato, A. and Rizzuti, L., (1989). The twin-system approach to experimental determination of residence time distributions, *Chem. Eng. Journal*, **42**, 73-82.

5. Brucato, A., Micale, G., Rizzuti, L., (1997). Determination of the amount of unsuspended solid particles inside stirred tanks by means of pressure measurements, *Rec Progr Genie des Proc*, **11**, 3-10.

6. Micale, G., Grisafi, F., Brucato, A., (2002). Assessment of particle suspension conditions in stirred vessels by means of a Pressure Gauge Technique, *Chem. Eng. Res. Des.*, **80**, 893-902.

7. Kee, R.C.S. and Tan, R.B.H., (2002). CFD simulation of solids suspension in mixing vessels. *Can. J. Chem. Eng.*, **80**, 721-726.

8. Ochieng, A. and Lewis, A.E., (2006). CFD simulation of solids off-bottom suspension and cloud height. *Hydrometallurgy*, **82**, 1-12.

9. Murthy, B.N., Ghadge, R.S. and Joshi, J.B., (2007). CFD simulations of gas-liquid-solid stirred reactor: prediction of critical impeller speed for solid suspension. *Chem. Eng. Sci.*, **62**, 7184-7195.

10. Kasat, G. R.; Khopkar, A. R.; Ranade, V. V. and Pandit, A. B, (2008). CFD Simulation of Liquid-Phase Mixing in Solid-Liquid Stirred Reactor. *Chem. Eng. Sci.*, **63**, 3877-3885.

11. Panneerselvam, R., Savithri, S. and Surender, G.D., (2008). CFD modeling of gas-liquid-solid mechanically agitated contactor. *Chem. Eng. Res. Des.*, **86**, 1331-1344.

12. Hosseini S., Patel D., Ein-Mozaffari F. and Mehrvar M., (2010). Study of solid-liquid mixing in agitated tanks through computational fluid dynamics modelling. *Ind. Eng. Chem. Res.*, **49**, 4426-4435.

13. Tamburini, A., (2011). *Suspension phenomena in solid-liquid agitated systems*, Chapter 4, Fotograf: Palermo, Italy - ISBN: 9788895272979.

14. Ljungqvist, M., Rasmuson, A., (2001). Numerical Simulation of the Two-Phase Flow In an Axially Stirred Vessels, *Chem. Eng. Res. and Des.*, **79**, 533-546.

15. Tamburini, A., Cipollina, A., Micale, G., Ciofalo, M. and Brucato, A., (2009). Dense solid–liquid off-bottom suspension dynamics: simulation and experiment. *Chem. Eng. Res. Des.*, **87**, 587–597.

16. Clift, R., Grace, J.R. and Weber, M.E., (1978). *Bubbles, drops and particles*. Academic Press, New York, San Francisco, London.

17. Brucato, A., Grisafi, F. and Montante, G., (1998). Particle Drag Coefficients in Turbulent Fluids, *Chem. Eng. Sci.*, **53**, 3295-3314.

18. Pinelli, D., Nocentini, M. and Magelli, F., (2001). Solids distribution in stirred slurry reactors: Influence of some mixer configurations and limits to the applicability of a simple model for predictions. *Chem. Eng. Sci.*, **188**, 91-107.

19. Zwietering T. N., (1958). Suspending of solid particles in liquids by agitators, *Chem. Eng. Sci.*, **8**, 244-253.